In situ investigation of copper corrosion in acidic chloride solution using atomic force – scanning electrochemical microscopy

J. Izquierdo[1,2], A. Eifert[1], C. Kranz[1,*], R.M. Souto[2,3,*]

[1] *Institute of Analytical and Bioanalytical Chemistry, University of Ulm, Albert-Einstein-Allee 11, D-89081 Ulm, Germany.*

[2] *Department of Chemistry, Universidad de La Laguna, P.O. Box 456, E-38200 La Laguna, Tenerife, Canary Islands, Spain.*

[3] *Institute of Material Science and Nanotechnology, Universidad de La Laguna, E-38200 La Laguna (Tenerife), Spain.*

Abstract

The anodic dissolution of pure copper surfaces in acidic chloride solution has been monitored in-situ using combined atomic force – scanning electrochemical microscopy (AFM-SECM). Here, the initial studies performed on model copper-modified substrates have been extended to the investigation of bulk copper samples used in industrial settings. The local release of Cu^{2+} ions was monitored through electrochemical reduction and deposition of the metal ions on the conductive frame of the AFM-SECM probe. Simultaneous monitoring of the topographical changes due to the corrosion process allowed the distinction and correlation of local passivation and pitting phenomena. The extent of the attack was estimated by anodic stripping of the copper metal deposited at the probe.

Keywords: AFM-SECM, copper corrosion, SG-TC mode, tip-integrated gold electrodes.

1. Introduction

Copper is among the most widely used metallic materials in industry with extensive application in electronics and heat exchangers. This metal exhibits high resistance towards corrosion upon exposure to most aqueous environments, thanks to the patina of multi-layered oxides spontaneously formed on its surface [1–4]. However, this passive layer undergoes local degradation in the presence of chloride containing environments, in particular under acidic conditions. The investigation of copper corrosion has thus been a topic of interest in material sciences for decades aiming to better predict and prevent its degradation. Most of our knowledge about the passive, active and metastable regimes of copper and copper-based alloys in various media (especially chloride and sulphate-containing environments) has been gained using electrochemical methods [3,5–13]. For example, monitoring of the open circuit potential (OCP) evolution allows the investigation of the nobility of the surface [6–10,12], whereas the protectiveness and self-healing ability of the passive layer is generally studied with dynamic polarization [6,9,10]. Electrochemical impedance spectroscopy provides additional information on the stability and structure of the passive film [7,8,12,13]. Statistical analysis of the current transients recorded under potentiostatic control permits the evaluation of the probability of transient degradation-repassivation phenomena below stable pitting conditions [5,11]. These electrochemical studies are frequently supported by ex-situ high-resolution microscopic observations, using e.g. scanning electron microscopy (SEM), in order to better discern the morphology and post-mortem appearance of the metal after exposure to the aggressive media [3,6–9,12]. In addition, the analysis of the surface composition with surface sensitive analytical techniques (e.g., Raman, energy-dispersive X-ray, or Auger electron spectroscopy) provides information on the composition and the structure of the formed patinas [8,9,12]. In particular, protection procedures against breakdown of copper-based materials in chloride-containing environments are often designed and tested using a combination of electrochemical and spectroscopic methods. Breakdown is frequently explained in terms of the formation of multilayers of copper chlorides, copper oxides and hydroxides, which are poorly adherent in the presence of chloride ions, resulting in the local degradation and dissolution of the unstable copper (I) chloride (CuCl) in aqueous solution [1,3,6,9,10,13].

However, the in-situ information collected by using the above-mentioned electrochemical methods average the response of the whole investigated surface, thus reflecting an average behavior from all the micrometer-sized active spots, and the remaining inactive areas. Hence, in order to discern the actually localized processes occurring at corroding metals, spatially resolved techniques operating under in-situ conditions are a prerequisite. Several scanning microelectrochemical techniques have been applied in corrosion science [14,15]. As a result, phenomena closely related to the active corrosion and protection of copper and copper-based alloys have been visualized using scanning Kelvin probe (SKP) [16], localized electrochemical impedance spectroscopy (LEIS) [17], scanning vibrating electrode technique (SVET) [18], or scanning tunneling microscopy [19,20]. In addition, scanning electrochemical microscopy (SECM) has been regarded as a particularly promising tool for the examination of corroding metals [21]. This is motivated by its ability to determine the concentration profiles of redox species of interest and their interaction with the metal surface [22,23]. In SECM, an ultramicroelectrode (UME) is used as probe, typically reassembling an electroactive micro-disc (10-25 µm diameter) made of glassy carbon or noble metal embedded in glass, which is positioned for electrochemical analysis in an electrolytic media in close vicinity to the sample surface. The recorded probe current response may reflect the interaction of (un)intentionally added redox

species with the surface (i.e., feedback mode) [24–26], and/or their consumption due to heterogeneous electrochemical processes (i.e., competition mode) [25,27]. In particular, SECM in the feedback mode has been recently employed to characterize the effect of grain orientation in the local electrochemical activity of copper [26]. Another particularly interesting SECM operation mode in corrosion science is the so-called substrate generation-tip collection (SG/TC) mode. In SG/TG mode redox active species are generated at the substrate surface and diffuse towards the tip, thus allowing the monitoring of the local release of metal cations from anodically active spots [21,28,29]. Thus, platinum and gold UMEs have been used as SECM probes to investigate Cu(II)-releasing surfaces like copper-based materials undergoing corrosion [30,31]. The quantitative electroanalytical determination of the bulk content of Cu^{2+} ions in aqueous environments has been achieved by using a gold UME [32,33], and it involves under-potential deposition (UPD) followed by anodic stripping. The visualization and determination of Cu^{2+} ion distributions released from corroding copper substrates using these procedures at the SECM is, thus, a very attractive method for the investigation of copper corrosion and protection.

Since SECM in constant height mode, rastering the tip in constant height in the *X,Y* plane, is not only sensitive to the electrochemical behavior of the conductive substrate, but may also be influenced by its morphology (in particular for sub-microsized SECM probes), complex responses may be obtained, where distinction of the various participating processes is not straightforward. In order to overcome this limitation, several strategies have been proposed [34]. Such strategies include shear-force mode SECM to maintain the tip-surface distance constant [35,36], or the use of alternating current SECM mode (AC-SECM), which may be used for 4-dimensional mapping [37,38]. An alternate route for the distinction of morphological features and electrochemical phenomena occurring on electrochemically active surfaces is the combination of SECM with complementary scanning probe techniques such as scanning ion conductance microscopy [39–41] or atomic force microscopy (AFM) [42,43]. Combined AFM-SECM was first employed in corrosion science for the monitoring of light alloys presenting intermetallic particles on their surface [44–46], and more recently for the electrochemical induction of localized pitting corrosion on otherwise passive metals [47,48]. Besides, while typically employed UMEs in SECM may reach spatial resolution in the order of few micrometers, the integration of conductive micro/nanoelectrodes at AFM probes make the sub-micrometric range readily accessible for SECM signals [49].

We have recently reported a novel microelectrochemical strategy for the visualization of copper anodic dissolution at model samples (Cu deposited on gold substrates) using an AFM-SECM probe fabricated from commercially available AFM probe with a gold square frame electrode and a silicon nitride thorn (AFM tip) [50]. The reduction and subsequent collection of Cu^{2+} ions released from copper-modified gold substrate at the AFM-tip integrated gold electrode probe was successfully correlated with the topographical changes resulting from the metal dissolution process. Semi-quantitative information was extracted from the anodic stripping of the collected ions in bulk solution. In the present work, the combined AFM-SECM approach has been extended to the characterization of a polycrystalline pure copper sample while subjected to increasing anodic polarization, in order to visualize topographical changes simultaneously to the detection of the released copper that was collected at the AFM-SECM probe, and later redissolved by anodic stripping voltammetry performed with the probe retracted to bulk solution.

2. Experimental section

Sodium chloride and copper sulphate of analytical grade were purchased from Merck (Darmstadt, Germany), and dissolved in ultrapure water (Elga water system, resistivity 18.0 MΩ cm; Elga Labwater, VWS Deutschland GmbH, Celle, Germany). Acid solutions were prepared by adjusting the pH with the addition of a very small amount of concentrated hydrochloric acid (VWR, Radnor, PA, USA), as to keep the total chloride concentration almost constant. All the experiments were carried out at room temperature (approximately, 20 ºC).

Copper samples of 99.99% purity were purchased as 1 mm thick sheets from Goodfellow (Cambridge, UK). They were cut into 2.5 cm x 2.5 cm square specimens, manually ground with silicon carbide papers of increasing grit from 220 to 4000, and subsequently mechanically polished with silica colloid micropolish suspension (0.05 µm particle size) in ultrapure water to produce a mirror-like finish. The polished surface was thoroughly rinsed with ultrapure water, immersed in ethanol and sonicated for 20 min in an ultrasonic bath for cleaning and degreasing, and finally dried under argon flow.

Prior to the actual AFM-SECM experiments, Tafel polarization tests were performed. Polished copper samples were mounted facing up in an adapted sandwich-like cell of approximately 1 mL total volume. Leakage was prevented with a 2 cm diameter o-ring. A platinum ring and an Ag/AgCl/KCl (sat.) were used as auxiliary and reference electrodes, respectively. All potentials in this work are referred to the Ag/AgCl/KCl (sat.) reference electrode. The three-electrode cell was connected to a CH660A potentiostat (CH Instruments, Austin, TX, USA), and Tafel polarization was done at 1 mV s^{-1} sweep rate from -0.50 to -0.12 V. Tafel polarization experiments were replicated four times.

The fabrication of the AFM-SECM probe has been already described in detail [49]. In brief, commercial silicon nitride cantilevers were modified with a layer of sputtered gold, followed by chemical vapor deposition of a silicon nitride layer. Next, cantilevers were re-shaped using a focus ion beam (FIB) system (Quanta 3D Dual Beam system from FEI, Eindhoven, NL), in order to expose a recessed gold square frame electrode surface and re-shape a sharp AFM tip. The dimensions of the integrated frame electrodes (thickness of the gold layer 100 nm) varied in terms of electrode edge length among the used probes. AFM-SECM measurements were done using combined probes with 1020 nm edge length for the gold frame, and 420 nm for the AFM tip. Electrical connections of the AFM-SECM probes and subsequent re-insulation of the contact point were achieved using conductive silver epoxy (PLANO GmbH, Wetzlar, Germany) and UV-sensitive glue (Dymax, Torrington, CT, USA), respectively.

For the quantitative evaluation of the tip response towards the electro-reduction of Cu^{2+} ions, AFM-SECM probes were mounted in a custom-built holder to immerse them in 0.5 M NaCl solution acidified to pH = 3, and connected as working electrodes to the CH660A potentiostat, completing the three-electrode configuration cell with a platinum ring counter-electrode and an Ag/AgCl/KCl (sat.) reference electrode. Then, calibration series were done by a deposition-stripping method with increasing additions of 0.10 M $CuSO_4$, covering the concentration range from 9.9 to 69.3 µM. The cathodic polarization stage was first done at -0.40 V during 256 seconds, and next linear sweep voltammetry (LSV) was performed at 50 mV s^{-1}. For calibration purposes, the integrated area of the voltammetric peak observed in the -0.20 to 0.10 V potential window was considered.

Two different workstations were used for the AFM-SECM experiments. At first, electrochemical control was performed using the in-built potentiostat of an atomic force microscopy with a SECM module from Keysight Technologies (Santa Rosa, CA, USA). The sensitivity of this instrument limits the current range of the sensing probe to ±100 nA, thus the recorded current reaches saturation beyond this range. Next, in order to further explore the potential and the limitations of the combined AFM-SECM technique, an external bipotentiostat from CH Instruments (CH832A) was used in another experimental series. In both cases, unless otherwise stated the AFM-SECM probe was connected as working electrode #1, the copper sample as working electrode #2, whereas a chlorinated silver wire and a platinum wire were employed as pseudo-reference and counter-electrode, respectively. The use of the external CH832A bipotentiostat imposed that the copper surface could not be maintained under potentiostatic control at all times, since the cell had to be intermittently switched off in order to change the potential of the working electrodes. The potential of the pseudo-reference electrode was measured versus a reference Ag/AgCl/KCl (sat.) in 0.5 M NaCl (pH = 3) test solution both before and after the experiments, resulting in ca. 48 mV, which is in good agreement with the theoretical value.

During the AFM-SECM measurements, two different constant potential values were applied to the substrate and the probe, aiming to control the release of copper cations from the copper sample and their redeposition at the combined probe. In this manner, the sample was immersed in the test solution of 0.5 M NaCl (pH = 3) and immediately polarized at -0.45 V. Next, the tip was also biased at -0.45 V in order to detect locally and collect the eventual release of Cu^{2+} ions while scanning the probe across the copper sample. AFM-SECM measurements were conducted over a randomly chosen area with a pixel resolution of 256 × 256. The copper surface was scanned at progressively increasing anodic substrate potential with varying increasing steps, where the smallest steps of 10 mV were adopted in the potential interval between -0.25 and -0.07 V. In a first series of experiments, the same region of dimensions 25 µm × 25 µm was scanned at 30 µm s^{-1}. When smaller areas of 5 µm × 5 µm or 2.5 µm × 2.5 µm dimensions were scanned at 6 µm s^{-1}, the drift in the piezoelectric motors did not allow to image precisely the same area of study. Roughness values were determined according to ISO 25178 norm to obtain values of the root mean square (rms) height. Immediately after each AFM-SECM measurement, the tip was withdrawn into the bulk solution, and the amount of copper that was deposited during the scan at the gold frame electrode of the AFM-SECM probe was reoxidized and redissolved. A withdrawal distance of 80 µm distance for copper redissolution was chosen for experiments were the 25 µm × 25 µm area was to be scanned, in order to ensure that the same area was maintained. Reoxidation in these experiments was conducted by cycling the potential applied at the tip at 50 mV s^{-1} between -0.45 and 0.45 V, which allowed to electrochemically characterize the electrolyte at still close distance from the surface (i.e. detect the copper ions releasing from the whole surface). In contrast, the maintenance of the same area for the scan acquisition was not possible along the sequence when scanning 5 µm × 5 µm or 2.5 µm × 2.5 µm regions. Hence, there was no need to stay close to the surface during the stripping of copper, and a larger withdrawal distance of 500 µm was used instead with reoxidation conducted potentiostatically at +0.45 V tip potential. During these stripping measurements, the substrate potential was maintained at the same value applied during the previous scan acquisition.

Scanning electron microscopy images and energy-dispersive X-ray spectroscopy measurements (SEM/EDS) were taken after from the copper surfaces after the polarization sequence and rinsing with water for the removal of remaining NaCl. For this purpose, the same Quanta 3D Dual Beam

system from FEI equipment, previously mentioned for FIB re-shaping of the AFM-SECM probes, was used.

3. Results and discussion

3.1 SECM probe and copper substrate electrochemical response in bulk solution

The stripping peaks of copper recorded at the AFM-SECM probes for various concentration of copper sulphate in test electrolyte was evaluated for the calibration of the electrochemical response of the tip-integrated gold electrode as shown in **Figure 1**. The duration of the copper deposition time at -0.40 V (namely, 256 s) was selected to match the approximate time needed to scan an area of the chosen dimensions at the selected scan rate. Anodic signals were registered during the anodic stripping of the deposited copper between -0.20 and +0.10 V, exhibiting a good correlation with the added copper content in solution in the micromolar range. It was previously observed that the stripping signals recorded with combined AFM-SECM probes for the reoxidation of a bulk copper deposit, can be employed to determine the amount of Cu^{2+} species released from copper deposits on gold [50]. Conversely, the anodic signal that is expected to occur at higher potentials (i.e., in the interval between 0.30 and 0.40 V), corresponding to the under-potential deposition of a copper monolayer on the gold electrode, is very small at these microelectrode surfaces, and it could not be used for quantitative purposes. Even in some cases when additional anodic signals were observed over 0.05 V, possibly due to the reoxidation of copper still remaining in contact with the gold (49.5 μM $CuSO_4$ concentration in Figure 1), those signals were not reproducible and therefore were not considered due to insuficient reliability.

The electrochemical behavior of pure copper upon increasing the anodic polarization was first tested with Tafel experiments. **Figure 2** depicts a typical polarization plot obtained in these conditions. The current response in the cathodic potential range is under diffusion-control for oxygen reduction, as evidenced by a high cathodic Tafel slope (291 ± 140 mV $decade^{-1}$), compared to the anodic slope (75.9 ± 6.3 mV $decade^{-1}$). No onset of hydrogen evolution reaction is expected to occur in this potential window in these electrolyte [51]. The corrosion potential (E_{corr}) was -0.220 ± 0.014 V, and the corrosion current density for the freely corroding copper, 14.2 ± 7.2 μA cm^{-2}, was determined from the intersection of the extrapolated Tafel slopes at this E_{corr}. Further extrapolation of the anodic Tafel line until -0.25 V (i,e, a cathodic overvoltage of -30 mV), shows that an anodic current density of 5.92 ± 3.28 μA cm^{-2} is still producing the release of a significant amount of copper ions. This is illustrated in Figure 2 by drawing blue dashed lines, being the Tafel experiment in Figure 2 the replicate measurement which provided the greatest current for this extrapolation. Since the current estimated from the Tafel experiments is an average measurement resulting from the total area of the copper sample, a geometric factor must be considered regarding the actual AFM-SECM measurements. That is, the combined microelectrode probe will exclusively collect the copper ions from the portion of the surface below its gold frame, namely, 1020 nm × 1020 nm. That is, from the copper released at this rate of 5.92 μA per square centimeter ($5.92 \cdot 10^{-6}$ C s^{-1} cm^{-2}) only a fraction of 1020 nm × 1020 nm area ($1.04 \cdot 10^{-8}$ cm^2) will eventually be sensed at the probe meanwhile. by applying the Faraday Law, it is possible to estimate the average release of copper, n_{Cu} from this smaller area. Accordingly, it is envisaged that an average release of 3.19×10^{-19} mol of Cu^{2+} per second will occur below the SECM active electrode while the surface is scanned during those measurements. This metal release will result in an increase in copper concentration in the volume confined below

the SECM integrated electrode. The simplest estimation of this volume would consider the cube defined by the 1020 nm × 1020 nm area below the gold frame and the 420 nm height of the topographic tip, resulting in a volume of $4.37 \cdot 10^{-16}$ L. By taking into account this small volume, the release of copper at that potential corresponds to 1.23×10^{-3} mol L^{-1} s^{-1}, and it woul be therefore measurable at the sensing probe. Although diffusion and accumulation phenomena should be taken into account in order to adequately determine the concentration of Cu^{2+} eventually present below the sensing probe during scanning, a rough correlation of the minimum current densities required to clearly register electrochemical information from the corrosion process may be envisaged with these calculations, as will be discussed below.

3.2 Corrosion behavior of copper

A selection of the AFM topographical images recorded during an experimental series involving 25 μm x 25 μm area scans, in which the copper sample was polarized at increasing anodic polarizations, is given in **Figure 3**, whereas **Figure 4** displays the simultaneously acquired SECM response. Software-based leveling correction was applied to the AFM images for the sake of comparison. A predominantly flat surface was observed when copper was polarized at potentials negative in respect to the E_{corr}, as illustrated in Figure 3A for the case of the substrate held at -0.35 V. The occurrence of some distinct topographical features (for instance, the hollow site located close to the center position) served to ensure that the same area was imaged during subsequent measurements. No significant SECM current was observed at the probe when the copper sample was subjected to cathodic polarization, as it can be seen in Figure 4A. Next, when the substrate potential was increased up to -0.18 and -0.16 V, some crystals appeared in the upper part of the AFM image (cf. Figures 3B and C). Meanwhile the hollow site, observed at a more negative potential value, disappeared progressively, possibly due to becoming filled with corrosion products and/or the slow dissolution of the complete surface. Those morphological observations reflect the initial stages of the corrosion process, with dynamic evolution of the passive layer occurring on the still mostly flat surface. Concurrently, the probe current response showed the electro-reduction of metal cations released from various spots of the anodically polarized copper surface (cf. Figures 4B and C). Tip current saturation beyond -100 nA occurred specially during the application of -0.16 V to the substrate, therefore it is only possible to detect the local production of copper, whereas local quantification becomes impossible at this stage. Interestingly, it was observed that the release of Cu^{2+} species was locally hindered at surface sites, where crystals were observed in the AFM maps: a fact evidenced by the zero current values recorded over those spots in the corresponding SECM images. Those crystals are probably the result of the accumulation and precipitation of poorly adherent copper salts. The chemical composition of these crystals remains unclear at this stage, though CuCl can be a potential candidate [1,3,6]. Chloride has been detected in the elemental composition of copper corrosion products and patinas formed after different corrosion tests in solutions only containing chloride as aggressive species, including acidic [52,53] and neutral [54,55] environments. In contrast, other authors have not found evidences of chloride incorporation into the passive layer even after long exposure to the chloride-containing solution [56,57]. Given the high dependence of the conditions for the corrosion test in the final composition of the passive layer, SEM images and EDS measurements of the copper surfaces were taken after the corrosion tests described herein in order to provide insights in the composition of the observed copper salts. SEM image in **Figure 5** reflects the morphology of the attacked copper surface. White salts are seen on top of the dark regions, which exhibit several holes due to the pitting process. Though EDS measurements were focused on both

the white precipitates and the dark regions, no signal of chloride was detected. Instead, only copper and oxygen were clearly observed, although displaying different ratios for each region (along with some carbon from contamination). Measurements on the white precipitates resulted in Cu/O atomic ratio 14.9 ± 8.5 (N = 6), whereas the oxygen content decreased significantly at the dark regions, where Cu/O ratio reached 34.3 ± 17.7 (N = 6). Therefore, apparently only copper oxides and hydroxides are formed in these acidic conditions, and no copper chloride is likely to be formed. This correlates well with information from literature, since CuCl has so far only been detected under neutral or acidic conditions [1,3,6].

The evolution of the unstable copper salts and oxide layer was evident in following AFM scans visible by the morphological changes occurring between Figure 3C (substrate potential -0.16 V) and 3D (-0.14 V). The surface becomes visibly corrugated, including small pits at several locations. More interestingly, the previously discussed growth of crystals was observed to progress when comparing these two AFM images. These features were still associated to the measurement of local SECM currents close to zero while the surrounding sample was mostly electrochemically active (cf. Figure 4D). Finally, active copper corrosion was clearly visualized when copper was further anodically polarized, as displayed in Figures 3E and F for substrate polarizations at -0.11 and -0.09 V, respectively. The previously observed crystals attributed to poorly adherent copper salts were not visible anymore, and dynamic degradation of the surface concurred at a highly heterogeneous surface (take notice that scales in Figures 3E and F progressively reflects larger height alterations), with the eventual formation of a propagating pit, visible in Figure 3F. The occurrence of a vigorous corrosion process was also visible with SECM, evidencing the generalized release of Cu^{2+} ions (cf. Figures 4E and F). Though the SECM current was found to be smaller in absolute values when the substrate was polarized at -0.09 V, the whole scanned area showed to be anodically activated, regardless the topographic features.

Quantitative information on the morphological evolution of the surface and the generation of Cu^{2+} species was extracted from the scans in Figures 3 and 4. This information is displayed in **Figure 6** as a function of the potentials applied to the substrate. It gives both the change of the surface roughness (black squares, left axis), and the total charge transferred through the AFM-SECM probe during the electro-reduction of copper for each scan (red circles, right axis). The total charge transferred was estimated by the total sum of all the current data points in the scan multiplied by the average time required to collect each data point. Roughness data were determined using AFM raw data (prior to any leveling correction), and hence reflect the thickening and eventual breakdown of the passive layer. On the other hand, the recorded charge indicates the extent of the corrosive attack from the anodically active sites detected at the surface. Substrate polarization above -0.22 V was required to record a significant metal release from SECM data, which reflects the application of a potential value more positive than the E_{corr} of copper in the electrolyte, determined from the Tafel experiment. Around this potential, changes in roughness started to occur, initially exhibiting a slow decrease, down to a minimum value coincident with the AFM image in Figure 3C, and next a significant increase in the roughness parameter. This evolution reflects the dynamic processes occurring at the passive layer under increasingly aggressive conditions, eventually resulting in both precipitation of corrosion products and local dissolution. As the driving force for anodic dissolution increases, the passive layer becomes smoother since the corrosion products show a tendency to fill the interstitial spaces (i.e. the spaces between grains and the metastable pits previously nucleated and already repassivated), yet increasing the applied potential results in the breakdown of the passive layer. At high anodic polarization (i.e., at -0.10 V), the charge monitored at the probe reached saturation (characterized by the current maximum

of the amplifier) due to the fact that the whole area was experiencing relatively high anodic dissolution, a feature also reflected by the further increase of surface roughness. The persisten dynamic evolution and activation-passivation of the formed pits at the most anodic potential, still below the active passive transition [51], is reflected by the variaations of surface roughness, which transitorily decrease at -0.08 V.

A selection of the anodic stripping voltammograms recorded at the probe is given in **Figure 7A**. The AFM-SECM probe was retracted from the sample to a distance of 80 µm, and the electrode was cycled between -0.45 and 0.45 V in order to ensure total copper redissolution from the electrode. Only the reoxidation measurements following scans recorded over the substrate polarized positive or equal to -0.25 V resulted in the appearance of a distinct anodic current peak between -0.20 and 0.10 V (see inset in Figure 7A). As discussed before, this minimum substrate potential of -0.25 V gives rise to an anodic current density of 10 µA cm^{-2} from the extrapolation of the anodic Tafel slope in Figure 2. Hence, this current density is regarded as the minimum anodic current due to the copper oxidation half-reaction of the corrosion process that could be observed as a distinguishable integrated AFM-SECM electrode signal using AFM-SECM. The area of the voltammetric peak obtained for the reoxidation of copper, after recording the AFM-SECM scan at a substrate potential of -0.25 V, amounted 5.02 pA · V, which accounts for the electrochemical conversion of $5.20 \cdot 10^{-16}$ moles of copper during reoxidation. As discussed before for the Tafel experiments (Figure 2), the same substrate potential of -0.25 V yields a production of $5.39 \cdot 10^{-19}$ mol of Cu^{2+} per second from an area located below the gold frame electrode of the AFM-SECM probe. Considering the time required to complete an AFM-SECM image (410 s), this would reflect a total release of $2.21 \cdot 10^{-16}$ moles of copper as deduced from the Tafel experiments, which is comparable with results obtained from reoxidation data in Figure 7A. The difference between the estimated copper release can be explained considering the different behavior of the copper substrate under potentiodynamic (Tafel experiments) and potentiostatic (AFM-SECM scans) conditions, as well as the capability of the tip to further collect diffusing copper ions from areas close to those being imaged, in particular while scanning the tip across the copper surface. As the anodic substrate potential is further increased, the height of the stripping voltammetric peak in Figure 7A consequently increases. Finally, current saturation occurs above +100 nA, a situation reached when copper is further polarized at potential values more anodic than -0.10 V (not shown).

Another feature can be distinguished from the voltammograms shown in Figure 7A. As the tip was only withdrawn 80 µm into bulk solution, it still remained close enough to the copper surface to sense some collection of copper ions from the dissolving surface (i.e., surface generation – tip collection mode). In fact, the potential applied to the substrate during the acquisition of the AFM-SECM scan was still maintained while the reoxidation voltammogram, presented in Figure 7A, was recorded. Thus, copper cations were still being released from the surface and were diffusing into bulk solution. Hence, during the cyclic voltammograms displayed in this figure, the cathodic scan down to a tip potential of -0.45 V allowed the electro-reduction of a portion of these diffusing copper ions. Consequently, a cathodic tip current response is recorded at tip potential values below -0.10 V, attaining diffusion-limited conditions at around -0.30 V as evidenced by the plateau observed for the cathodic current below this value. As expected, the absolute value of that current increases as the anodic potential applied to the substrate is increased, due to the faster anodic dissolution of copper.

Figure 7B displays the effect of substrate polarization on the integrated peak area and the cathodic diffusion current values obtained for all the reoxidation curves in Figure 7A (including those

where current saturation was reached during the anodic stripping). The inset in Figure 7B shows the trend followed by the data at substrate potential more negative than -0.15 V. An exponential response is observed for both parameters from the beginning of the experimental series, reflecting the expected exponential increase of the copper anodic dissolution with the applied substrate potential. A relative minimum value of the peak area was found at -0.10 V substrate polarization. Conversely, the cathodic diffusion limiting currents maintain the tendency towards higher cathodic values along this substrate potential interval. Whereas the copper stripping is mostly related to the previous collection of copper during the AFM-SECM scan acquisition over the confined 25 μm × 25 μm area under consideration, the cathodic current resulting from the detection of copper at 80 μm distance reflects the averaged release of metal cations from much larger areas. Hence, this fact suggests that the considered scanned area may be partially deactivated (i.e., passivated) and thus less copper is collected while scanning, but the anodic dissolution of the whole substrate is enhanced, consequently detecting increasing copper cations after tip withdrawal.

3.3 Local detection of pit degradation phenomena

The above described methodology and results demonstrates the applicability of AFM-SECM for the observation of the general trends in the 25 μm x 25 μm selected surface area, reflecting the corrosion behavior of copper at the micrometer scale. However, given the lateral resolution of the technique, the proposed methodology has the potential to be further exploited in the investigation of more localized phenomena in the sub-micrometer range. Besides, the use of the external bipotentiostat may partially avoid the current saturation observed in previously discussed experiments. In addition, for the local investigation it is necessary to avoid or discern the copper detection in the cathodic potential values in Figure 7, which results from the general copper release and diffusion into bulk solution. The latest requires the anodic stripping to be performed at further distances from the substrate and/or using a potentiostatic method. In this section, the results of AFM-SECM experimental series performed following such requirements with the use of the external CH-832a bipotentiostat described in the experimental section will be discussed.

The initial stages in the generation of a single pit could be detected by collecting the AFM-SECM measurements given in Figure 8. AFM image in Figure 8A was obtained with copper sample polarized at -0.24 V, that is, below the corrosion potential, and the 5 μm x 5 μm image exhibits a mostly flat surface with some distinct features as apparent holes below 1μm diameter. Such holes may be attributed to the development of metastable pitting corrosion, most likely in between the scan acquisition due to the unavoidable intermittent interruption of the potentiostatic control of the sample, as mentioned in the experimental section. Indeed, the evaluated surface roughness, given in Table 1, exhibits an increasing tendency, although this trend cannot be taken as evidence since the imaged area was not maintained exactly the same along the experimental sequence. Table 1 also displays the charge obtained in potentiostatic mode during the reoxidation of the copper from the integrated electrode at 500 μm distance from the surface once scans were finished, finding no relevant variations up to this substrate potential of -0.24 V.

During the scan acquisition at substrate potential -0.22 V in Figure 8B, several observations from the AFM image suggested the activation of the copper surface. As the scans were acquired from bottom to top, initial lines gave no relevant alteration of the surface up to the $Y = 1.75\ \mu m$. Then, the acquisition of the surface morphology became dramatically disturbed, and a pit hole of ca. 0.5

μm in diameter (irregular shape) is eventually seen in the upper part of the AFM scan, whereas surface roughness increased thrice (from 3.14 to 9.19 nm, see Table 1). At the same time, the SECM scan depicted in Figure 8C showed probe current evolution from this $Y = 1.75\ \mu m$ position. Although the tip current saturation was not limited up to 1 μA with the sensitivity in use during the scan, the dark blue areas in Figure 8C (below -10 nA in the color scale) reached this saturation level in almost all cases. The limitations of the methodology are, thus, not completely overcome by the use of the external potentiostat, since the local release of copper and its accumulation in the confined volume below the tip apparently results in an excess of copper accumulation. However, the more localized evaluation of the surface permitted the distinction of active areas around the pit initiated in the upper part of the scanned area. Considering that the square gold frame SECM electrode is 1 μm long each side, the detection of Cu^{2+} is more likely to occur when the topographically sensitive thorn is moving around the apparently active 0.5 μm hole. In addition, the signal obtained during the redissolution of the copper from the integrated electrode resulted in a 8-fold increment when compared to the previous measurement (from 17.3 to 141 nC, see Table 1). Finally, background SECM current was distinctly increased in the nA range during the last lines of the scan in Figure 8C (where the pit was seen in Figure 8B), also reflecting the activation of the corrosion phenomena.

Subsequent scans conducted at more positive potential, up to -0.20 V in Figure 8D, did not provide unambiguous local electrochemical information (SECM image not shown), and only the surface roughness was observed to decrease down to 4.15 nm, suggesting the deactivation of the area under investigation. Once finished this series, the probe was again approached to the sample surface and copper was subjected to an anodic polarization sweep at 1 mV s^{-1} while the AFM-SECM tip rastered a 2.5 μm x 2.5 μm area at 1 μm s^{-1}, polarized at -0.45 V. The resulting current for both working electrodes is displayed in Figure 9. After all the polarization sequence, the corrosion potential of the copper sample is shifted to -0.104 V, reflected by the transition from cathodic to anodic current values. Shortly after, the probe current experiences an increment in the cathodic direction between -0.076 and 0.064 V, reflecting the release and detection of copper and immediate deactivation of the surface. Finally, when the substrate potential is above -0.050 V, the probe cathodic current is dramatically increased due to the intensity of the attack.

4. Conclusions

Copper corrosion was monitored in acidic chloride solutions in respect to topography changes and electrochemical signals as a function of substrate potential, with sub-micrometer spatial resolution, using combined AFM-SECM. The tip assembly herein employed allowed the correlation of the accumulation of corrosion products with the local passivation they provide, evidenced by the absence of copper cations over those sites. The dynamics of passive layer formation and breakdown has been characterized in terms of the surface roughness evolution, reflecting its initial growth and subsequent breakdown and pit formation. This is accompanied by the progressive activation of the copper surface and Cu(II) production, as locally detected by the AFM tip-integrated electrode. Anodic copper dissolution was detected even below the E_{corr} in the acidified chloride solution, evidenced by the local detection and collection of copper and its subsequent reoxidation from the AFM-SECM probe retracted to the bulk solution. The strategy outlined here is regarded feasible for application to other metallic substrates undergoing corrosion, thus opening a new route for the elucidation of the still uncertain aspects of corrosion mechanisms of a wide variety of materials.

Acknowledgements

R.M.S. and J.I. acknowledge the Spanish Ministry of Economy and Competitiveness (MINECO, Madrid, Spain) and the European Regional Development Fund (Brussels, Belgium), under grants CTQ2012-36787 and CTQ2016-80522-P. A Research Training Grant awarded to J.I. by MINECO (*Programa de Formación de Personal Investigador*) is gratefully acknowledged. Short stay scholarships awarded to J.I. by the German Service of Academic Exchange (DAAD), and by the University of La Laguna are thanked. The Focused Ion Beam Center UUlm, which is supported by FEI Company (Eindhoven, The Netherlands), the German Science Foundation (INST40/385-F1UG), and the Struktur- und Innovationsfonds Baden-Württemberg (Germany) are greatly acknowledged.

5. References

[1] G. Mankowski, J.P. Duthil, A. Giusti, The pit morphology on copper in chloride- and sulphate-containing solutions, Corros. Sci. 39 (1997) 27–42. doi:10.1016/S0010-938X(96)00100-X.

[2] S. González, M. Pérez, M. Barrera, A.R. González-Elipe, R.M. Souto, Mechanism of copper passivation in aqueous sodium carbonate−bicarbonate solution derived from combined X-ray photoelectron spectroscopic and electrochemical data, J. Phys. Chem. B. 102 (1998) 5483–5489. doi:10.1021/jp981069k.

[3] S. Sathiyanarayanan, M. Sahre, W. Kautek, In-situ grazing incidence X-ray diffractometry observation of pitting corrosion of copper in chloride solutions, Corros. Sci. 41 (1999) 1899–1909. doi:10.1016/S0010-938X(99)00021-9.

[4] R. Procaccini, W.H. Schreiner, M. Vázquez, S. Ceré, Surface study of films formed on copper and brass at open circuit potential, Appl. Surf. Sci. 268 (2013) 171–178. doi:10.1016/j.apsusc.2012.12.050.

[5] C. Monticelli, G. Trabanelli, G. Meszaros, Investigation on copper corrosion behaviour in industrial waters by electrochemical noise analysis, J. Appl. Electrochem. 28 (1998) 963–969. doi:10.1023/A:1003401128653.

[6] J.P. Ferreira, J.A. Rodrigues, I.T.E. da Fonseca, Copper corrosion in buffered and non-buffered synthetic seawater: A comparative study, J. Solid State Electrochem. 8 (2004) 260–271. doi:10.1007/s10008-003-0445-1.

[7] A. Srivastava, R. Balasubramaniam, Electrochemical impedance spectroscopy study of surface films formed on copper in aqueous environments, Mater. Corros. 56 (2005) 611–618. doi:10.1002/maco.200503866.

[8] Y. Van Ingelgem, A. Hubin, J. Vereecken, Investigation of the first stages of the localized corrosion of pure copper combining EIS, FE-SEM and FE-AES, Electrochim. Acta. 52 (2007) 7642–7650. doi:10.1016/j.electacta.2006.12.039.

[9] A.M. Alfantazi, T.M. Ahmed, D. Tromans, Corrosion behavior of copper alloys in chloride media, Mater. Des. 30 (2009) 2425–2430. doi:10.1016/j.matdes.2008.10.015.

[10] M. Antonijevic, S. Alagic, M. Petrovic, M. Radovanovic, A. Stamenkovic, The influence of pH on electrochemical behavior of copper in presence of chloride ions, Int. J.

Electrochem. Sci. 4 (2009) 516–524. doi:http://www.electrochemsci.org/papers/vol4/4040516.pdf.

[11] A.-M. Lafront, F. Safizadeh, E. Ghali, G. Houlachi, Study of the copper anode passivation by electrochemical noise analysis using spectral and wavelet transforms, Electrochim. Acta. 55 (2010) 2505–2512. doi:10.1016/j.electacta.2009.12.006.

[12] H. Ha, C. Taxen, K. Williams, J. Scully, Effects of selected water chemistry variables on copper pitting propagation in potable water, Electrochim. Acta. 56 (2011) 6165–6183. doi:10.1016/j.electacta.2011.04.008.

[13] I. Betova, M. Bojinov, C. Lilja, Influence of chloride on the long-term interaction of copper with deoxygenated neutral aqueous solutions, Corros. Sci. 76 (2013) 192–205. doi:10.1016/j.corsci.2013.06.043.

[14] P. Marcus, F. Mansfeld, Analytical methods in corrosion science and engineering, CRC Press, Boca Raton, 2006.

[15] R. Oltra, V. Maurice, R. Akid, P. Marcus, Local probe techniques for corrosion research, Woodhead Publishing Ltd, Cambridge, 2007.

[16] D. Nakhaie, A. Davoodi, A. Imani, The role of constituent phases on corrosion initiation of NiAl bronze in acidic media studied by SEM-EDS, AFM and SKPFM, Corros. Sci. 80 (2014) 104–110. doi:10.1016/j.corsci.2013.11.017.

[17] M. Sánchez, N. Aouina, D. Rose, P. Rousseau, H. Takenouti, V. Vivier, Assessment of the electrochemical microcell geometry by local electrochemical impedance spectroscopy of copper corrosion, Electrochim. Acta. 62 (2012) 276–281. doi:10.1016/j.electacta.2011.12.041.

[18] J. Izquierdo, J.J. Santana, S. González, R.M. Souto, Scanning microelectrochemical characterization of the anti-corrosion performance of inhibitor films formed by 2-mercaptobenzimidazole on copper, Prog. Org. Coatings. 74 (2012) 526–533. doi:10.1016/j.porgcoat.2012.01.019.

[19] E. Martinez-Lombardia, V. Maurice, L. Lapeire, I. De Graeve, K. Verbeken, L. Kestens, P. Marcus, H. Terryn, In Situ Scanning Tunneling Microscopy Study of Grain-Dependent Corrosion on Micrystalline Copper, J. Phys. Chem. C. 118 (2014) 25421–25428. doi:10.1039/a906140a.

[20] H. Chen, M. Bettayeb, V. Maurice, L.H. Klein, L. Lapeire, K. Verbeken, H. Terryn, P. Marcus, Local passivation of metals at grain boundaries: In situ scanning tunneling microscopy study on copper, Corros. Sci. 111 (2016) 659–666. doi:10.1016/j.corsci.2016.04.013.

[21] A.C. Bastos, A.M. Simões, S. González, Y. González-García, R.M. Souto, Imaging concentration profiles of redox-active species in open-circuit corrosion processes with the scanning electrochemical microscope, Electrochem. Commun. 6 (2004) 1212–1215. doi:10.1016/j.elecom.2004.09.022.

[22] L. Niu, Y. Yin, W. Guo, M. Lu, R. Qin, S. Chen, Application of scanning electrochemical microscope in the study of corrosion of metals, J. Mater. Sci. 44 (2009) 4511–4521. doi:10.1007/s10853-009-3654-x.

[23] M.B. Jensen, D.E. Tallman, Application of SECM to corrosion studies, in: A.J. Bard, C.G. Zoski (Eds.), Electroanal. Chem. a Ser. Adv., vol. 24, CRC Press, Boca Raton, 2012: p. 171.

[24] K. a. Ellis, M.D. Pritzker, T.Z. Fahidy, Modeling the degradation of scanning electrochemical microscope images due to surface roughness, Anal. Chem. 67 (1995) 4500–4507. doi:10.1021/ac00120a012.

[25] Y. González-García, S.J. García, A.E. Hughes, J.M.C. Mol, A combined redox-competition and negative-feedback SECM study of self-healing anticorrosive coatings, Electrochem. Commun. 13 (2011) 1094–1097. doi:10.1016/j.elecom.2011.07.009.

[26] E. Martinez-Lombardia, Y. Gonzalez-Garcia, L. Lapeire, I. De Graeve, K. Verbeken, L. Kestens, J.M.C. Mol, H. Terryn, Scanning electrochemical microscopy to study the effect of crystallographic orientation on the electrochemical activity of pure copper, Electrochim. Acta. 116 (2014) 89–96. doi:10.1016/j.electacta.2013.11.048.

[27] K. Eckhard, X. Chen, F. Turcu, W. Schuhmann, Redox competition mode of scanning electrochemical microscopy (RC-SECM) for visualisation of local catalytic activity, Phys. Chem. Chem. Phys. 8 (2006) 5359–5365. doi:10.1039/b609511a.

[28] K. Fushimi, M. Seo, An SECM observation of dissolution distribution of ferrous or ferric ion from a polycrystalline iron electrode, Electrochim. Acta. 47 (2001) 121–127. doi:10.1016/S0013-4686(01)00557-6.

[29] R.M. Souto, Y. González-García, D. Battistel, S. Daniele, In situ scanning electrochemical microscopy (SECM) detection of metal dissolution during zinc corrosion by means of mercury sphere-cap microelectrode tips, Chem. - A Eur. J. 18 (2012) 230–236. doi:10.1002/chem.201102325.

[30] D. Ruhlig, W. Schuhmann, Spatial imaging of Cu2+-ion release by combining alternating current and underpotential stripping mode scanning electrochemical microscopy, Electroanalysis. 19 (2007) 191–199. doi:10.1002/elan.200603693.

[31] A. Papaderakis, A.G. Anastopoulos, S. Sotiropoulos, Electrochemical studies of processes occurring at the polycrystalline Cu electrode/methanol interface, J. Electroanal. Chem. 783 (2016) 217–225. doi:10.1016/j.jelechem.2016.11.017.

[32] J. Zhuang, L. Zhang, W. Lu, D. Shen, R. Zhu, D. Pan, Determination of trace copper in water samples by anodic stripping voltammetry at gold microelectrode, Int. J. Electrochem. Sci. 6 (2011) 4690–4699. doi:http://www.electrochemsci.org/papers/vol6/6104690.pdf.

[33] A.P.R. de Souza, A.S. Lima, M.O. Salles, A.N. Nascimento, M. Bertotti, The use of a gold disc microelectrode for the determination of copper in human sweat, Talanta. 83 (2010) 167–170. doi:10.1016/j.talanta.2010.09.001.

[34] M.A. O'Connell, A.J. Wain, Combined electrochemical-topographical imaging: a critical review, Anal. Methods. 7 (2015) 6983–6999. doi:10.1039/C5AY00557D.

[35] M. Ludwig, C. Kranz, W. Schuhmann, H.E. Gaub, Topography feedback mechanism for the scanning electrochemical microscope based on hydrodynamic forces between tip and sample, Rev. Sci. Instrum. 66 (1995) 2857–2860. doi:10.1063/1.1145568.

[36] A. Hengstenberg, C. Kranz, W. Schuhmann, Facilitated tip-positioning and applications of non-electrode tips in scanning electrochemical microscopy using a shear force based constant-distance mode, Chemistry. 6 (2000) 1547–1554. doi:10.1002/(SICI)1521-3765(20000502)6:9<1547::AID-CHEM1547>3.3.CO;2-3.

[37] K. Eckhard, T. Erichsen, M. Stratmann, W. Schuhmann, Frequency-dependent alternating-current scanning electrochemical microscopy (4D AC-SECM) for local visualisation of corrosion sites, Chem. - A Eur. J. 14 (2008) 3968–3976.

doi:10.1002/chem.200701861.

[38] J. Izquierdo, S. González, R.M. Souto, Application of AC-SECM in corrosion science: Local visualization of heterogeneous chemical activity in AA2024 surfaces, Int. J. Electrochem. Sci. 7 (2012) 11377–11388. doi:http://www.electrochemsci.org/papers/vol7/71111377.pdf.

[39] D.J. Comstock, J.W. Elam, M.J. Pellin, M.C. Hersam, Integrated ultramicroelectrode-nanopipet probe for concurrent scanning electrochemical microscopy and scanning Ion conductance microscopy, Anal. Chem. 82 (2010) 1270–1276. doi:10.1021/ac902224q.

[40] Y. Takahashi, A.I. Shevchuk, P. Novak, Y. Murakami, H. Shiku, Y.E. Korchev, T. Matsue, Simultaneous noncontact topography and electrochemical imaging by SECM/SICM featuring ion current feedback regulation, J. Am. Chem. Soc. 132 (2010) 10118–10126. doi:10.1021/ja1029478.

[41] M.A. O'Connell, A.J. Wain, Mapping electroactivity at individual catalytic nanostructures using high-resolution scanning electrochemical-scanning ion conductance microcopy, Anal. Chem. 86 (2014) 12100–12107. doi:10.1021/ac502946q.

[42] J. V Macpherson, P.R. Unwin, Combined scanning electrochemical-atomic force microscopy, Anal. Chem. 72 (2000) 276–285. doi:10.1021/ac990921w.

[43] C. Kranz, Recent advancements in nanoelectrodes and nanopipettes used in combined scanning electrochemical microscopy techniques, Analyst. 139 (2014) 336–352. doi:10.1039/c3an01651j.

[44] A. Davoodi, J. Pan, C. Leygraf, S. Norgren, In situ investigation of localized corrosion of aluminum alloys in chloride solution using integrated EC-AFM/SECM techniques, Electrochem. Solid-State Lett. 8 (2005) B21. doi:10.1149/1.1911900.

[45] A. Davoodi, J. Pan, C. Leygraf, S. Norgren, Probing of local dissolution of Al-alloys in chloride solutions by AFM and SECM, Appl. Surf. Sci. 252 (2006) 5499–5503. doi:10.1016/j.apsusc.2005.12.023.

[46] A. Davoodi, J. Pan, C. Leygraf, S. Norgren, The role of intermetallic particles in localized corrosion of an aluminum alloy studied by SKPFM and integrated AFM/SECM, J. Electrochem. Soc. 155 (2008) C211. doi:10.1149/1.2883737.

[47] J. Izquierdo, A. Eifert, R.M. Souto, C. Kranz, Simultaneous pit generation and visualization of pit topography using combined atomic force–scanning electrochemical microscopy, Electrochem. Commun. 51 (2015) 15–18. doi:10.1016/j.elecom.2014.11.017.

[48] J. Izquierdo, A. Eifert, C. Kranz, R.M. Souto, In Situ Monitoring of Pit Nucleation and Growth at an Iron Passive Oxide Layer by using Combined Atomic Force and Scanning Electrochemical Microscopy, ChemElectroChem. 2 (2015) 1847–1856. doi:10.1002/celc.201500100.

[49] C. Kranz, G. Friedbacher, B. Mizaikofft, A. Lugstein, J. Smoliner, E. Bertagnolli, Integrating an ultramicroelectrode in an AFM cantilever: Combined technology for enhanced information, Anal. Chem. 73 (2001) 2491–2500. doi:10.1021/ac001099v.

[50] J. Izquierdo, B.M. Fernández-Pérez, A. Eifert, R.M. Souto, C. Kranz, Simultaneous atomic force – scanning electrochemical microscopy (AFM-SECM) imaging of copper dissolution, Electrochim. Acta. (2015). doi:10.1016/j.electacta.2015.12.160.

[51] A.V. Benedetti, P.T.A. Sumodjo, K. Nobe, P.L. Cabot, W.G. Proud, Electrochemical

studies of copper, and copper-aluminium-silver alloys: Impedance results in 0.5 M NaCl, Electrochim. Acta. 40 (1995) 2657–2668. doi:10.1016/0013-4686(95)00108-Q.

[52] E.M. Sherif, S.M. Park, Inhibition of copper corrosion in acidic pickling solutions by N-phenyl-1,4-phenylenediamine, Electrochim. Acta. 51 (2006) 4665–4673. doi:10.1016/j.electacta.2006.01.007.

[53] H. Gerengi, M. Mielniczek, G. Gece, M.M. Solomon, Experimental and Quantum Chemical Evaluation of 8-Hydroxyquinoline as a Corrosion Inhibitor for Copper in 0.1 M HCl, Ind. Eng. Chem. Res. 55 (2016) 9614–9624. doi:10.1021/acs.iecr.6b02414.

[54] E.S.M. Sherif, Effects of 2-amino-5-(ethylthio)-1,3,4-thiadiazole on copper corrosion as a corrosion inhibitor in 3% NaCl solutions, Appl. Surf. Sci. 252 (2006) 8615–8623. doi:10.1016/j.apsusc.2005.11.082.

[55] T. Kosec, D.K. Merl, I. Milošev, Impedance and XPS study of benzotriazole films formed on copper, copper-zinc alloys and zinc in chloride solution, Corros. Sci. 50 (2008) 1987–1997. doi:10.1016/j.corsci.2008.04.016.

[56] I. Milošev, N. Kovačević, J. Kovač, A. Kokalj, The roles of mercapto, benzene and methyl groups in the corrosion inhibition of imidazoles on copper: I. Experimental characterization, Corros. Sci. 98 (2015) 107–118. doi:10.1016/j.corsci.2015.05.006.

[57] W. Qafsaoui, M.W. Kendig, S. Joiret, H. Perrot, H. Takenouti, Ammonium pyrrolidine dithiocarbamate adsorption on copper surface in neutral chloride media, Corros. Sci. 106 (2016) 96–107. doi:10.1016/j.corsci.2016.01.029.

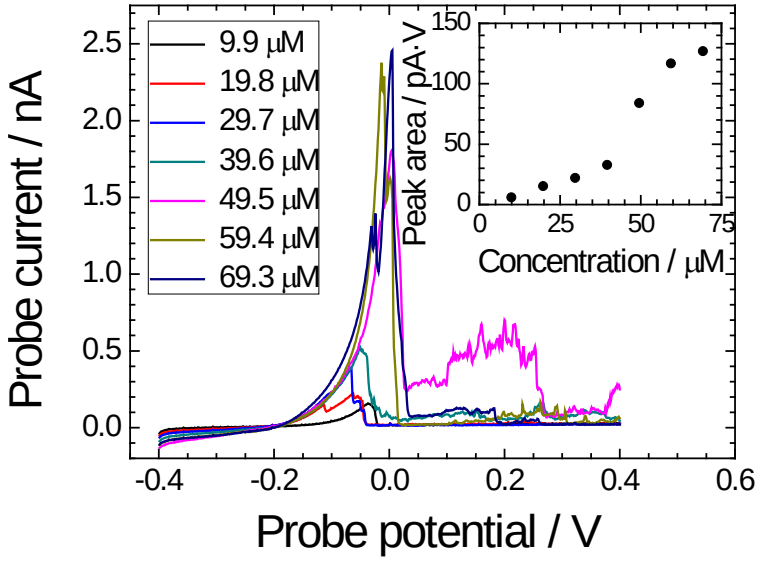

Figure 1. Anodic stripping voltammograms of the copper metal deposited onto the AFM-tip integrated probes for their calibration against the $CuSO_4$ concentration in 0.5 M NaCl (pH = 3) test solution. Inset shows the calibration plot obtained after integration of the voltammetric peak. Sweep rate: 50 mV s^{-1}. Metal deposition conditions: 256 s at -0.4 V.

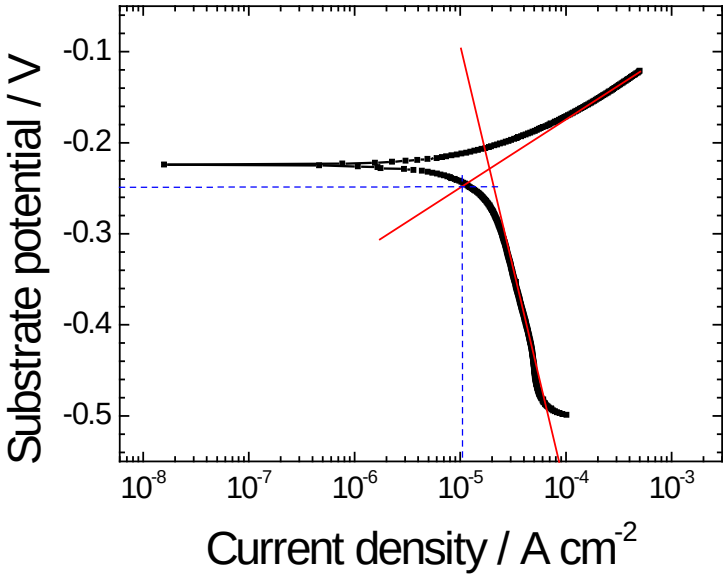

Figure 2. Tafel polarization of the copper sample in 0.5 M NaCl (pH = 3) solution recorded at 1 mV s^{-1}. Red lines represent the Tafel anodic and cathodic slopes. Dashed blue lines show the extrapolation of the anodic current for substrate potential -0.25 V.

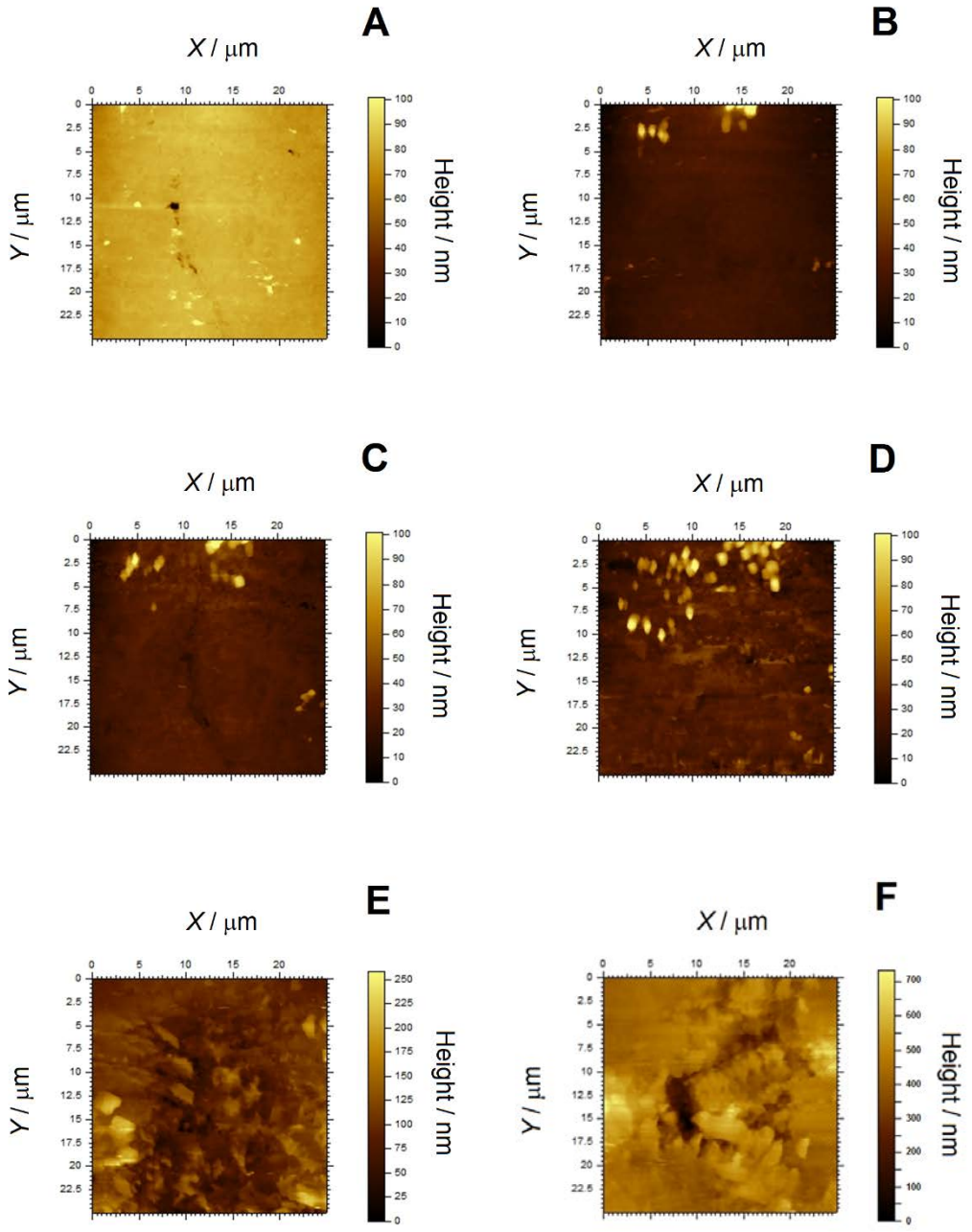

Figure 3. Selected AFM images recorded with the AFM-SECM probe over the same copper area, while polarized at (A) -0.35, (B) -0.18, (C) -0.16, (D) -0.14, (E) -0.11, and (F) -0.09 V.

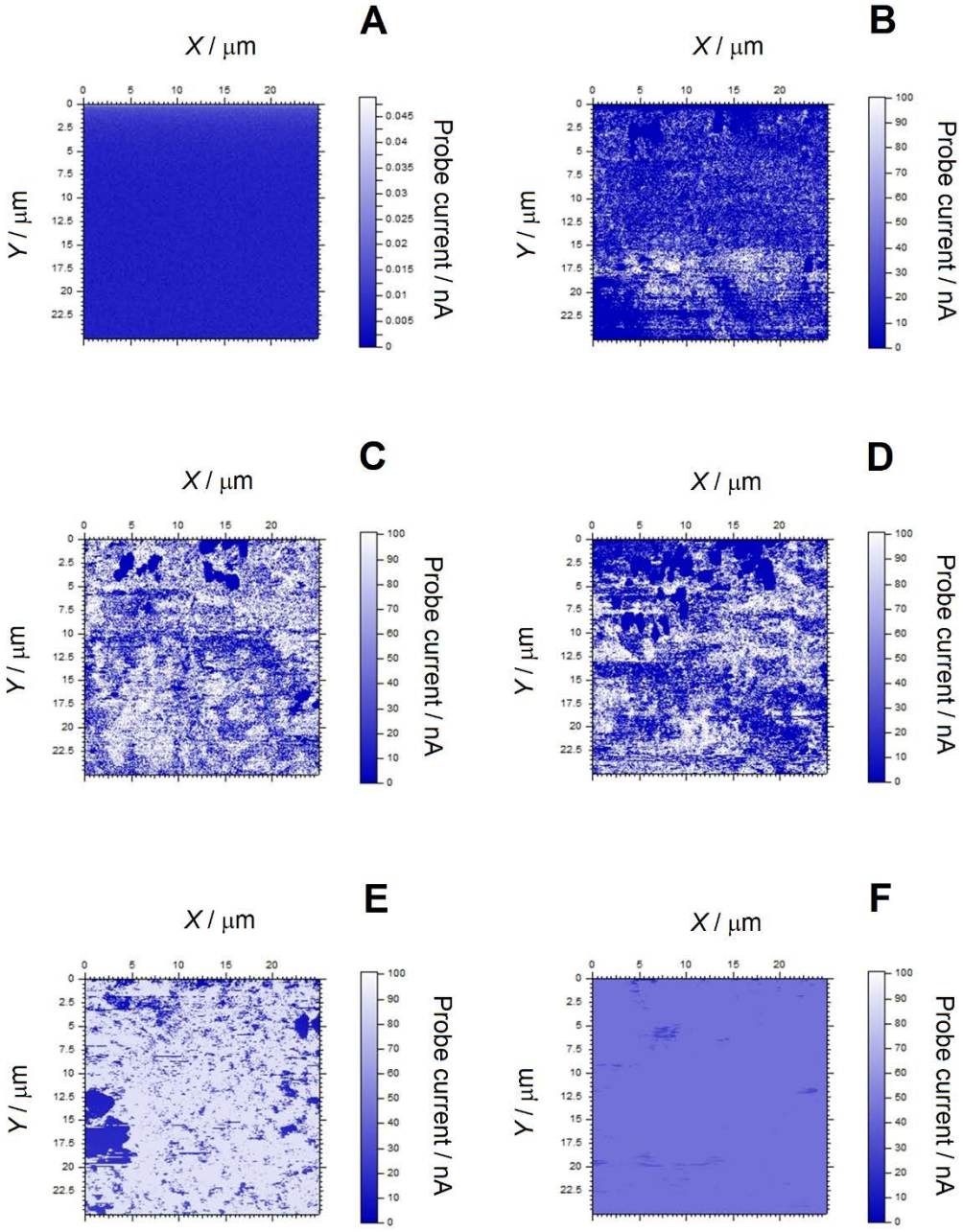

Figure 4. Selected SECM images recorded with the AFM-SECM probe over the same copper area, while polarized at (A) -0.35, (B) -0.18, (C) -0.16, (D) -0.14, (E) -0.11, and (F) -0.09 V. Potential of the AFM-SECM probe: -0.45 V.

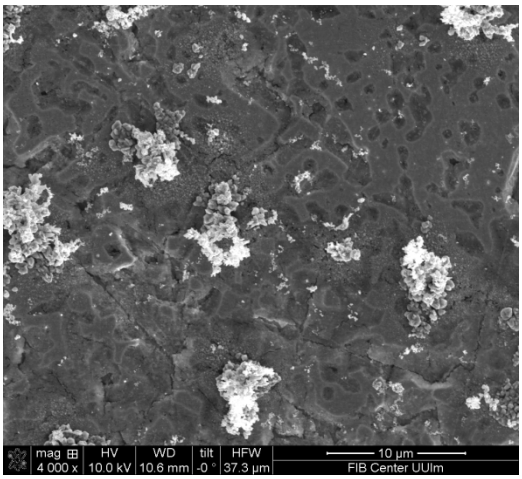

Figure 5. SEM image of the copper surface after the corrosion test was finished

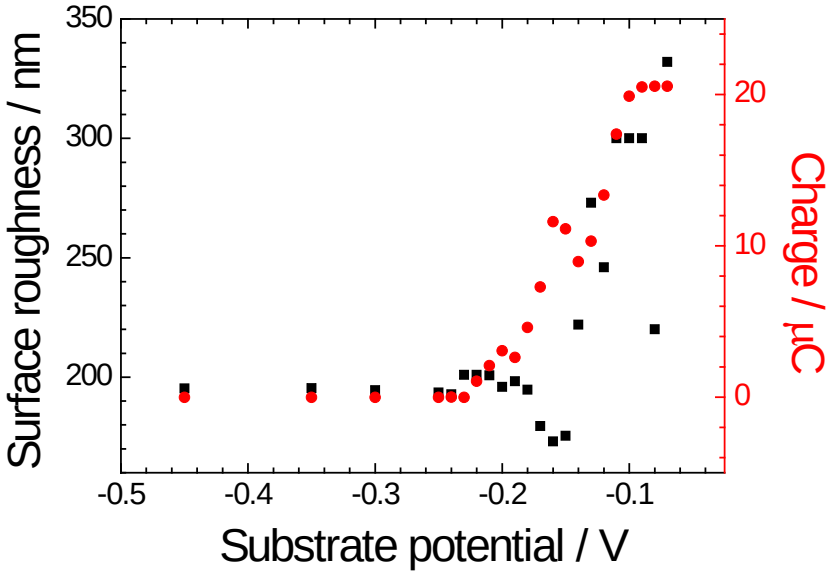

Figure 6. Effect of the applied substrate potential on the surface roughness and the faradaic charge transferred at the probe during the recording of the AFM-SECM images shown in Figure 4.

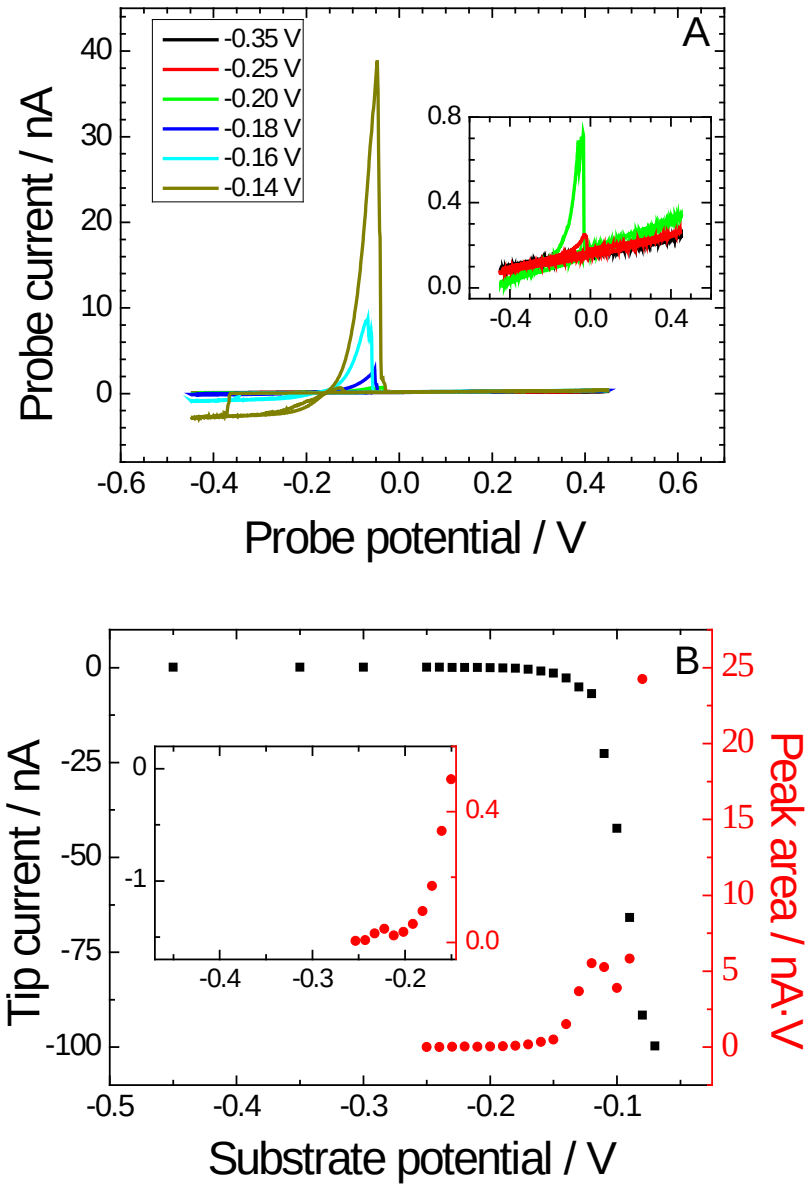

Figure 7. (A) Anodic stripping of the copper deposited at the AFM-SECM probe. Legend in the plot indicates the potential applied to the substrate during the acquisition of the previous AFM-SECM scan. Tip-substrate distance: 80 µm; sweep rate: 50 mV s^{-1}. (B) Limiting cathodic current obtained at the most negative tip potential of -0.45 V (black squares, left axis), and integrated peak area between -0.2 and 0.1 V (red circles, right axis), as a function of the potential applied to the substrate.

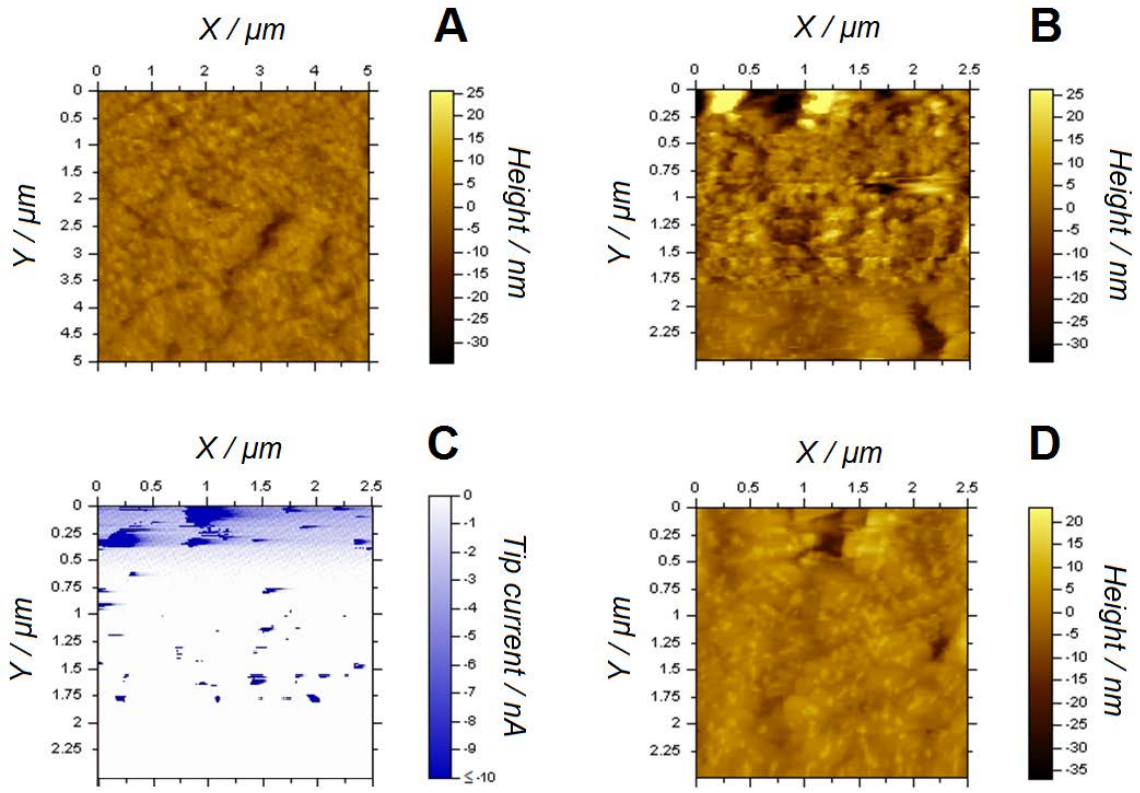

Figure 8. (A,B,D) AFM and (C) SECM images recorded with the AFM-SECM probe over a random copper area, while polarized at (A) -0.24, (B,C) -0.22, and (D) -0.20. Scan dimensions: (A) 5 µm x 5 µm, (B-C) 2.5 µm x 2.5 µm. Scan rate: 6 µm s^{-1}. Potential of the AFM-SECM probe: -0.45 V.

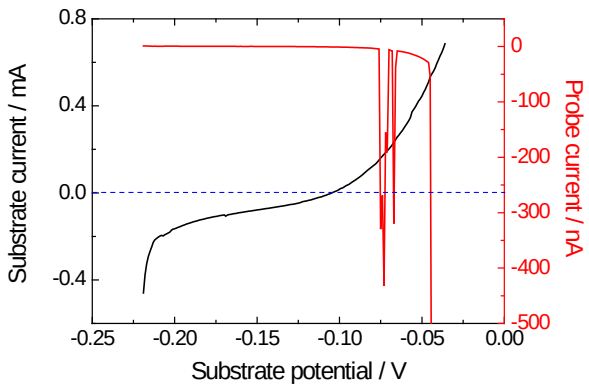

Figure 9. Current response of the copper substrate (black line, left axis) and AFM-SECM probe (red line, right axis) while performing anodic linear sweep voltammogram of the copper sample at 1 mV s^{-1}, after the experimental series seen in Figure 7 and Table 1. The potential of the AFM-SECM probe was maintained at -0.45 V with tip stationary in contact with the sample.

Table 1. Evolution of the surface roughness and reoxidation charge in experimental series discussed in Section 3.2

Substrate potential / V	rms / nm	Reoxidation charge / nC
-0.45	1.96	-
-0.30	2.03	8.47
-0.25	2.53	10.6
-0.24	3.58	10.1
-0.23	3.14	17.3
-0.22	9.19	141
-0.21	-	15.2
-0.20	4.15	6.68